

Supporting Information

Integrating machine learning and digital microfluidics for screening experimental conditions

Fatemeh Ahmadi,^{1,3} Mohammad Simchi,⁴ James M. Perry,² Stephane Frenette,² Habib Benali,^{1,2}
Jean Paul Soucy,^{2,5} Gassan Massarweh,⁵ Steve C. C. Shih *¹⁻³

¹ Department of Electrical and Computer Engineering, Concordia University, 1455 de
Maisonneuve Blvd. West, Montréal, Québec, Canada, H3G 1M8

² PERFORM Centre, Concordia University, 7200 Sherbrooke Street West, Montréal, Québec,
Canada, H4B 1R6

³ Centre for Applied Synthetic Biology, Concordia University, 7141 Sherbrooke Street West,
Montréal, Québec, Canada, H4B 1R6

⁴ Department of Mechanical & Industrial Engineering, University of Toronto, 5 King's College
Rd, Toronto, Ontario, Canada, M5S 3G8

⁵ McConnell Brain Imaging Centre, Montreal Neurological Institute, McGill University, 3801
University Street, Montréal, Québec, Canada, H3A 2B4

*Corresponding author

Tel: +1-(514) 848-2424 x7579

Email: steve.shih@concordia.ca

Table of Contents

Experimental Section.....	3
Radioisotope solution preparation	3
Radiotracer synthesis on-chip.....	3
Fabrication of the PDMS-based purifier disc	5
Temperature control module	5
Reagent delivery system.....	6
Analysis and QC test for the [¹⁸ F]FDG.	7
Supplementary tables	8
Table S1. Ten experiments for the traditional approach.....	8
Table S2. Experiments automated on DMF for the machine learning model database	9
Table S3. Specifications of the optimal on-chip synthesis	10
Supplementary figures	11
Figure S1: Digital microfluidic device design.....	11
Figure S2: Linear models based on single input.....	12
Figure S3: Performance of the linear models based on single input.	13
Figure S4: Modeling of the fluorination efficiency based only on significant factors. .	14
Figure S5: Testing droplet movement fidelity for the radiosynthesis chemicals.	15
Figure S6: On device purification of the fluorinated product by PDMS-based discs. ..	16
Figure S7: Temperature control module.....	17
Figure S8: Reagent delivery system.	18
Figure S9: Hardware and software.	19
References.....	20

Experimental Section

Radioisotope solution preparation

The [^{18}F]-fluoride solution was delivered in [^{18}O]-heavy water solution and [^{18}F]-fluoride was trapped on a quaternary methyl ammonium (QMA) cartridge. The QMA cartridge was primed with 10 mL of K_2CO_3 (125 mM) and 10 mL of distilled water. K_{222} (10 mg) was dissolved in the stock solution of K_2CO_3 (150 μL , 125 mM) and diluted in 1.35 mL of anhydrous MeCN to make the elution buffer. The [^{18}F]-fluoride was eluted from the QMA using the buffer and the generated [^{18}F]KF/ K_{222} complex was transferred into the syringe.

Radiotracer synthesis on-chip

We followed a protocol similar to Chen et al.⁶ Briefly, prior to operation, mannose triflate (1-4 mg) was dissolved in 100 μL of MeCN to form the precursor solution with concentrations ranging from 20- 80 mM. The [^{18}F] was obtained from the cyclotron (Montreal Neurological Institute, Montreal, Canada) with a radioactivity of 0.2 mCi. Sodium hydroxide (2 - 40 mg) was dissolved in 1 mL distilled water to make the deprotecting agent. A glass syringe was filled with the [^{18}F]KF/ K_{222} complex (see Supporting Information for radioisotope solution preparation). All synthesis reagents except for the [^{18}F] and MeCN were dispensed with a pipette onto the reagent reservoirs.

On-chip radiotracer synthesis for the random and OFAT approach were implemented in four steps. In step (1), the temperature of the thermoelectric element was set at 25 °C and 30 - 100 μL of the [^{18}F]KF/ K_{222} complex was flown through the tubing to one of the central electrodes in the reaction site. The droplet containing the complex was heated to 120 °C and held for 3 min to

evaporate the solvent. Next, in step (2), azeotropic drying were performed by adding MeCN (10-20 μL via syringe pump) to the dried residue at 120 $^{\circ}\text{C}$, incubated for 3 min, and repeated two additional times. The temperature of the reaction site was held at 120 $^{\circ}\text{C}$ for 1 min and then decreased to 25 $^{\circ}\text{C}$. In step (3), five droplets of mannose triflate solution (6 μL each) were gradually dispensed from a reagent reservoir and were added to the reaction site. The temperature was increased to 85 $^{\circ}\text{C}$ and held for 5 min at the reaction site. Finally, in step (4), from a separate reagent reservoir, a dispensed droplet of NaOH solution (10 μL , 0.05-1 M) was added to the mixture at 50 $^{\circ}\text{C}$ and the mixture was moved in circular paths for about 5 minutes to mix the solution. For downstream analysis of the sample quality, the ITO cover plate was removed, and the final mixture was removed from the device by adding 5 μL of water using a pipette (see Supporting Information for QC analysis).

To purify the [^{18}F]FDG product on-chip, the purifier disc (see **Figure S6** for disc fabrication) was preconditioned with 50:50 (v/v) ethanol/water solvent mixture and placed on top of one electrode (labeled ‘purifier disc spot’; **Figure S1**) prior to droplet operation. Following the droplet operation procedure (see above), the final [^{18}F]FDG solution (~ 30 μL) was moved across the purifier disc to remove the unreacted [^{18}F] fluoride from the product. After 20 - 40 min of holding the droplet over the disc, the ITO cover plate was removed and 10 μL of water was added to the disc by a pipette. Purified [^{18}F]FDG was collected from the disc into an Eppendorf for QC analysis (see Supporting Information for QC analysis).

Fabrication of the PDMS-based purifier disc

A novel PDMS-based purifier disc was designed for purifying the final radiolabeled product (**Figure S6**). After mixing the elastomer and the crosslinker (10:1) and degassing the PDMS, we

poured the mixture on a petri dish. The mixture was spin-coated on the petri dish (60 s – 500 rpm) yielding a 100- 120 μm PDMS layer. The volume of the PDMS mixture is determined based on the diameter of the petri dish used such that it makes a uniform layer from center to edge.

The PDMS was baked in an oven (70 $^{\circ}\text{C}$) for 2 hours. However, when the PDMS was half cured we poured alumina powder on top of the mixture to a final mass that it completely covers the surface and let the PDMS solidify for another hour. Once the PDMS is completely cured, we coated the layer with TeflonTM AF 1600 (1000 rpm for 1.5 min) to ease droplet transfer on top of the purifier disc. Then, we punched a circle in the PDMS layer and made 6 mm and 2 mm diameter purifier discs. The purifier disc was placed on the DMF device where we have expanded the area of the electrodes. The final product mixture was moved to this area onto the disc for purification.

Temperature control module

Heating (up to 120 $^{\circ}\text{C}$) and cooling (down to 25 $^{\circ}\text{C}$) of the reaction site was provided by a 14.8 \times 14.8 mm² thermoelectric device (Peltier, VT-31-1.0-1.3, TE technology inc., TX, USA), integrated below the DMF device for procedure related to evaporation and radiolabeling on chip (**Figure S7**). A same size (14.8 \times 14.8 mm²) aluminum heat-block with a 1.5 mm horizontal drilled hole at the center was placed between the TEC and the DMF chip. To enhance the heat transfer, a thin layer of thermal paste (GC electronics, Rockford, IL, USA) was applied between the device and TEC. For temperature control, a resistance temperature sensor (Building Automation Products, Inc., Gays Mills, WS, USA) was in the aluminum heat-block hole and secured in place with thermal paste. The Peltier was mounted to a 94 mm \times 82 mm integrated

heatsink and fan (12 V DC). A 3D printed holder was used to interface the heating module with the DMF device.

Reagent delivery system

The reagents used in microliter quantities are delivered to the chip by micropipettes. However, to load the radioisotope onto the device and reliably achieve sufficient volumes of radiotracer, we integrated a syringe pump delivery system to our DMF setup. The syringe pump was reproduced from an open-source 3D-printed model on Thingiverse website [See <https://www.thingiverse.com/thing:2812734>]. We have made some minor changes to the 3D model to be able to use the slider as a syringe holder (**Figure S8A**). The stepper motor is controlled by an Arduino microcontroller and the user can set the volume to be loaded onto the chip through the python-based code. The stepper motor was calibrated for the volume loaded in each step angle (**Figure S8B**).

A PEEK tubing (IDEX Yellow 1/16" OD x .007" ID, SciPro/ Scientific Products & Equipment, Oshawa, ON, Canada) was used to transfer the reagent from the syringe to the chip. The peek tubing is taped on the pogopin holder on top of the microfluidic chip. The loaded volume was monitored via a digital camera (EO-1312 Monochrome, Edmond Optics, Barrington, NJ, USA) mounted on top of the microfluidic device.

Analysis and QC test for the [¹⁸F]FDG.

Radioactivity recovery was calculated as the ratio of the radioactivity of collected crude product to starting radioactivity on the chip. This measurement was corrected for decay so that we achieve

the activity loss only due to manipulation. Fluorination efficiency of the crude product collected from the chip was determined via radio thin layer chromatography (radio-TLC). A 2 μ L droplet of the crude product was spotted on silica TLC plates. Once the TLC plate was dried in the air, it was developed in a mobile phase of 95 % acetonitrile and 5 % distilled water, and then analyzed with a scanner (MiniGITA star). Using the resulting chromatograms, the peak area of the [18 F]FDG peak was calculated and divided by the area of both [18 F]FDG and unreacted [18 F]fluoride peaks to obtain the fluorination efficiency. Crude radiochemical yield (crude RCY, decay-corrected) is defined as the radioactivity recovery times the fluorination efficiency. The purity of the radioisotope was measured with a gamma spectrometer using the same silica TLC plate with the crude sample spot.

Supplementary tables

Table S1. Ten experiments for the traditional approach

	Mannose triflate volume/ [¹⁸ F] volume	Mannose triflate concentration (mM)	Radiolabeling temperature (°C)	Radiolabeling time (min)	NaOH concentration (M)	Deprotection temperature (°C)	Deprotection time (min)	Fluorination Efficiency (%)
1	1.0	20	85	4	0.01	25	2	12.16
2	1.0	20	85	5	0.05	25	2	31.69
3	0.3	30	85	5	1.00	50	5	41.38
4	0.6	30	100	7	1.00	50	5	64.36
5	0.6	30	85	3	1.00	25	5	37.45
6	1.2	20	85	7	0.50	25	4	52.21
7	1.2	20	85	5	1.00	25	5	65.92
8	1.5	20	85	5	0.10	25	4	22.47
9	1.8	20	85	7	0.05	25	2	48.30
10	1.0	10	100	5	1.00	50	5	31.44

Table S2. Experiments automated on DMF for the machine learning model database

	Mannose triflate volume/ [¹⁸ F] volume	Mannose triflate concentration (mM)	Radiolabeling temperature (°C)	Radiolabeling time (min)	NaOH concentration (M)	Deprotection temperature (°C)	Deprotection time (min)	Fluorination Efficiency (%)	Rare condition
1	1.0	10	85	5	1.00	25	5	11.86	Yes
2	1.0	30	85	5	0.10	25	5	15.62	Yes
3	0.6	30	85	7	1.00	25	5	27.63	Yes
4	1.2	20	85	4	0.05	25	5	30.51	Yes
5	1.0	20	85	5	1.00	25	5	35.02	No
6	1.0	10	100	5	1.00	50	5	37.83	Yes
7	1.0	20	85	5	1.00	25	5	39.21	No
8	0.3	30	85	5	1.00	25	5	40.37	Yes
9	0.3	30	85	5	1.00	25	5	41.56	Yes
10	1.0	20	85	5	0.05	25	2	41.69	Yes
11	0.3	20	85	5	1.00	25	5	42.41	Yes
12	1.0	30	85	5	1.00	25	3	42.79	Yes
13	1.0	30	100	5	0.05	50	5	44.25	Yes
14	1.0	20	100	5	1.00	50	5	45.01	No
15	1.0	20	85	5	1.00	25	5	45.96	No
16	1.0	20	85	5	1.00	25	5	46.34	No
17	1.0	20	100	5	1.00	50	5	48.85	No
18	1.0	20	85	7	1.00	25	5	48.97	Yes
19	1.0	20	85	5	1.00	50	5	50.13	No
20	1.0	30	85	5	1.00	25	5	50.23	No
21	0.3	30	100	5	1.00	50	5	50.47	Yes
22	0.3	30	85	5	1.00	25	5	51.21	Yes
23	0.3	30	85	5	1.00	25	5	51.48	Yes
24	1.0	30	85	5	1.00	25	5	53.41	No
25	1.0	30	100	5	1.00	25	5	54.54	No
26	1.0	30	100	5	0.50	50	5	54.55	Yes
27	1.0	30	85	7	1.00	25	5	54.56	Yes
28	1.0	30	85	5	1.00	25	5	54.82	No
29	1.0	50	100	5	1.00	50	5	55.52	Yes
30	1.0	30	100	5	1.00	50	10	55.69	Yes
31	1.0	30	100	5	1.00	25	5	56.97	No
32	1.0	30	85	5	1.00	25	5	57.91	No
33	1.0	50	100	5	1.00	50	5	61.69	Yes
34	1.5	20	85	5	1.00	25	5	62.78	Yes
35	1.0	20	100	5	1.00	50	5	64.79	No
36	0.3	30	85	5	1.00	25	5	64.81	Yes
37	1.0	30	100	5	1.00	50	5	65.83	No
38	1.0	30	85	5	1.00	50	5	66.12	No
39	1.0	50	100	5	1.00	50	5	66.74	Yes
40	1.0	50	100	5	1.00	50	5	67.03	Yes
41	1.0	30	85	5	1.00	25	5	67.37	No
42	1.0	30	100	5	1.00	50	5	68.27	No
43	1.0	30	100	5	1.00	50	5	69.17	No
44	1.0	30	85	5	1.00	25	5	69.56	No
45	1.0	50	100	5	1.00	50	5	71.54	Yes
46	1.0	20	100	5	1.00	50	5	71.79	No
47	1.0	30	100	5	1.00	50	5	71.93	No
48	1.0	30	85	5	1.00	25	5	72.22	No
49	1.0	30	100	7	1.00	50	5	73.31	Yes
50	1.0	30	100	5	1.00	50	5	73.59	No
51	1.0	30	100	5	1.00	25	5	74.92	No
52	2.0	30	100	7	1.00	50	5	75.23	Yes
53	1.0	50	100	5	1.00	50	5	76.09	Yes
54	1.0	30	100	5	1.00	50	5	76.14	No
55	1.0	20	100	5	1.00	50	5	77.14	No

Table S3. Specifications of the optimal on-chip synthesis

Radioactivity recovery ^a	[¹⁸F]-incorporation ^b	Crude radiochemical yield ^c	Radionuclide purity ^d	Radiochemical purity ^e
94.1% ± 1.50 %	70.82% ± 1.54 %	66.64% ± 2.51 %	99.93 % ± 0.02 %	93.05 % ± 2.46 %

- a. The ratio of radioactivity of collected crude product to the starting radioactivity on the chip.
- b. The peak area of the [¹⁸F]FDG on the radio-TLC chromatogram divided by the area of [¹⁸F]FDG plus [¹⁸F] peaks.
- c. The radioactivity recovery times the fluorination efficiency.
- d. Purity of the radioisotope only.
- e. Chemical purity of [¹⁸F]FDG achieved with our PDMS-based disc purifier.

Supplementary figures

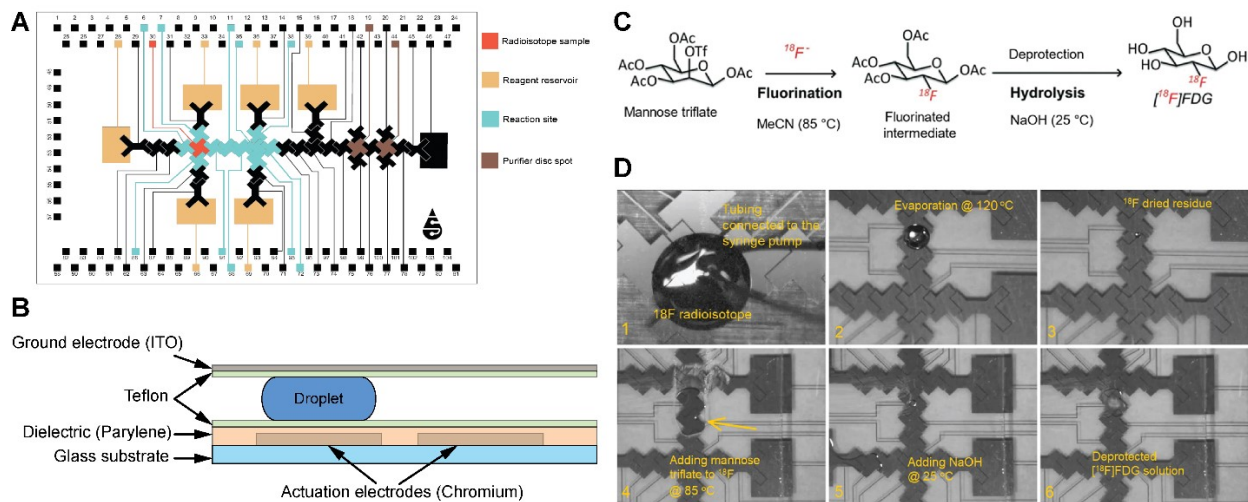


Figure S1: Digital microfluidic device design. (A) The schematic of the microfluidic device, illustrating the reservoir electrodes for $[^{18}F]KF/K_{222}$ complex and all other reagents. PDMS based purifier discs were also placed on the bottom plate on the indicated electrodes. (B) The structure of the digital microfluidic device. (C) Radiochemistry workflow on digital microfluidic device. (D) Frames 1-6 from a movie depicting the radiolabeling automation process on the DMF device.

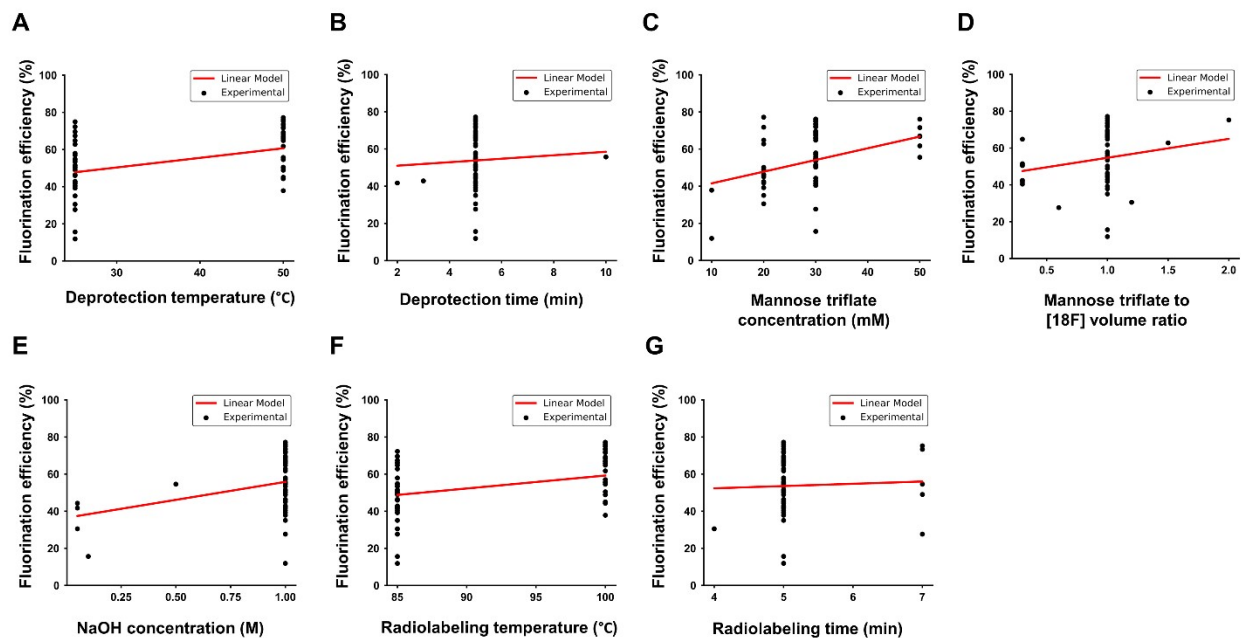


Figure S2: Linear models based on single input. (A-G) Linear regression model for all seven parameters that are related to fluorination efficiency. Values were selected based on previous work in the area (ref). The database (containing $n = 55$) in Table S2 was used to generate these linear single input models.

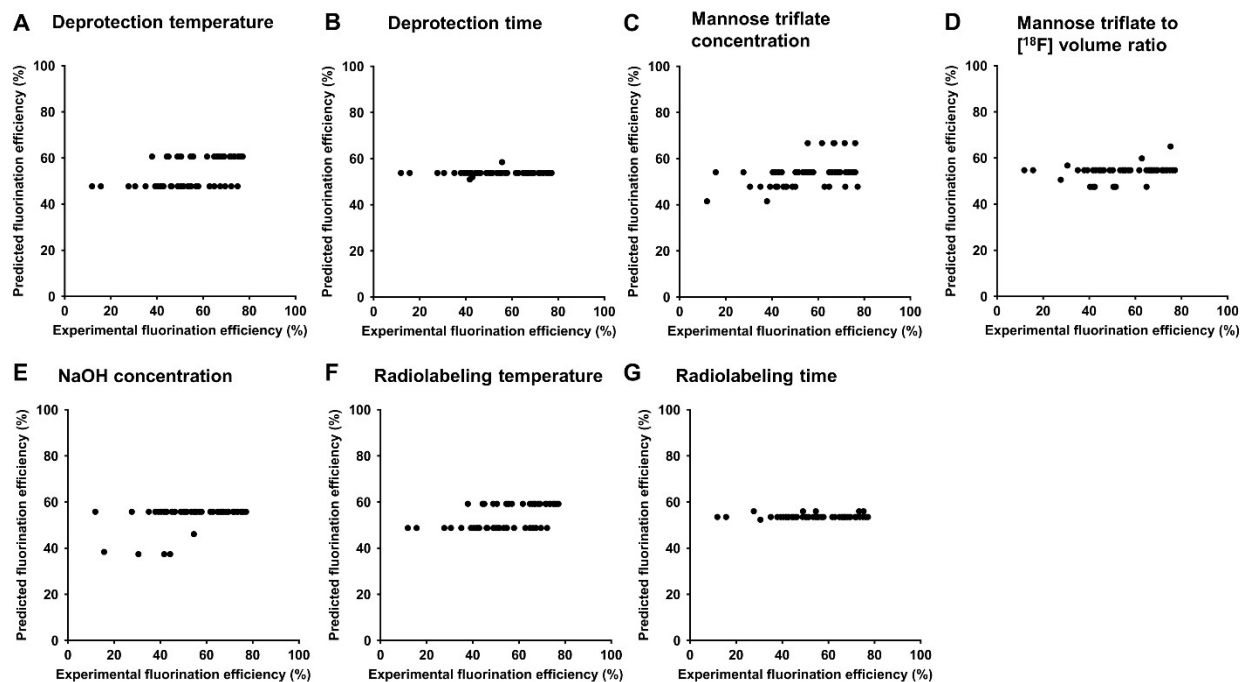


Figure S3: Performance of the linear models based on single input. (A-G) Assessment of the performance of the predicted fluorination efficiency using our model against the generated data set. The database from Table S2 ($n = 55$) was used to generate these models.

A

Parameter	Model's coefficient
NaOH concentration (M)	4.53
Deprotection time (min)	-0.75
Mannose triflate concentration (mM)	3.94
Radiolabelling temperature (°C)	4.39
Mannose triflate / ¹⁸ F volume ratio	2.61

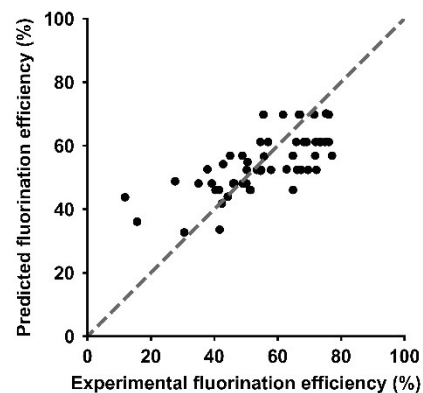
B

Figure S4: Modeling of the fluorination efficiency based only on significant factors. (A) Coefficients of the completed linear model for the five significant factors, which was used to predict the optimal fluorination efficiency. (B) Linear model performance with training and test RMSE values of 11.86 ± 2.3 and 11.99, respectively.

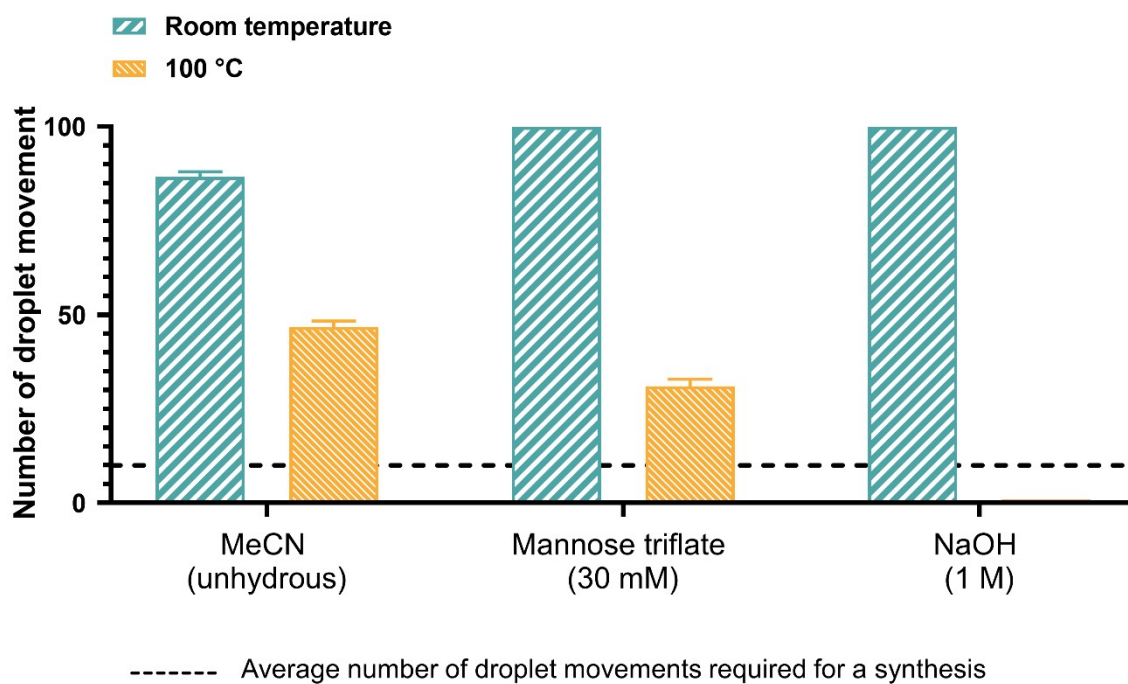


Figure S5: Testing droplet movement fidelity for the radiosynthesis chemicals. Three reagents (MeCN, mannose triflate, and NaOH) that are involved in the radiosynthesis of [^{18}F]FDG were evaluated for on-chip manipulation at two different temperature (25 °C and 100 °C). Droplet movements were repeated for each reagent (with certain concentrations needed for radiosynthesis) with voltages below 110 V_{rms} and 15 KHz frequency.

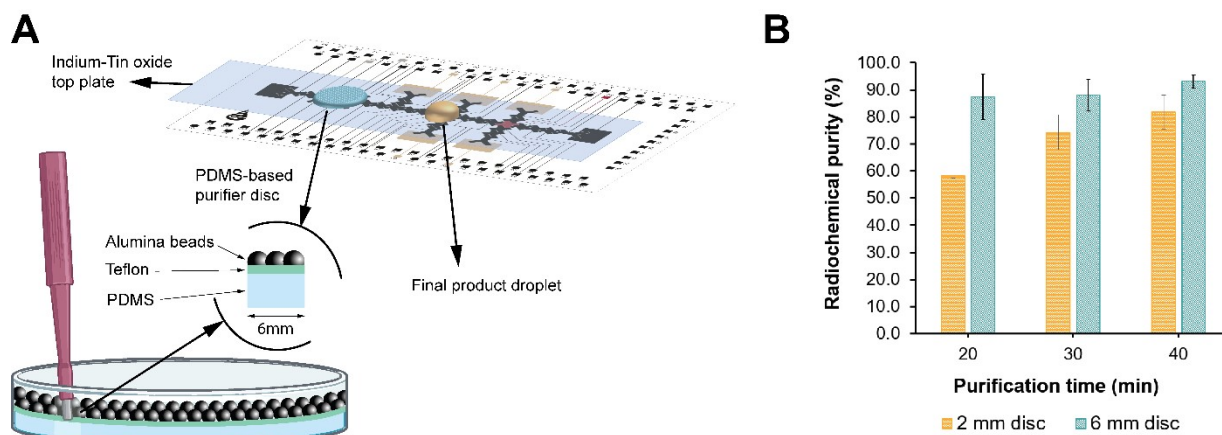


Figure S6: On device purification of the fluorinated product by PDMS-based discs. 2-mm or 6-mm PDMS-based discs were fabricated in a petri dish (see methods) and were punched using a puncher. The purifier disc was placed on the DMF device on the dedicated electrodes (see Figure S1) which was sandwiched between the top- and bottom-plates. The final product mixture was actuated to the disc and incubated for 20, 30, or 40 minutes. (B) The measured radiochemical purity as a function of purification time for 2-mm and 6-mm sized discs. All error bars show one standard deviation with three replicates.

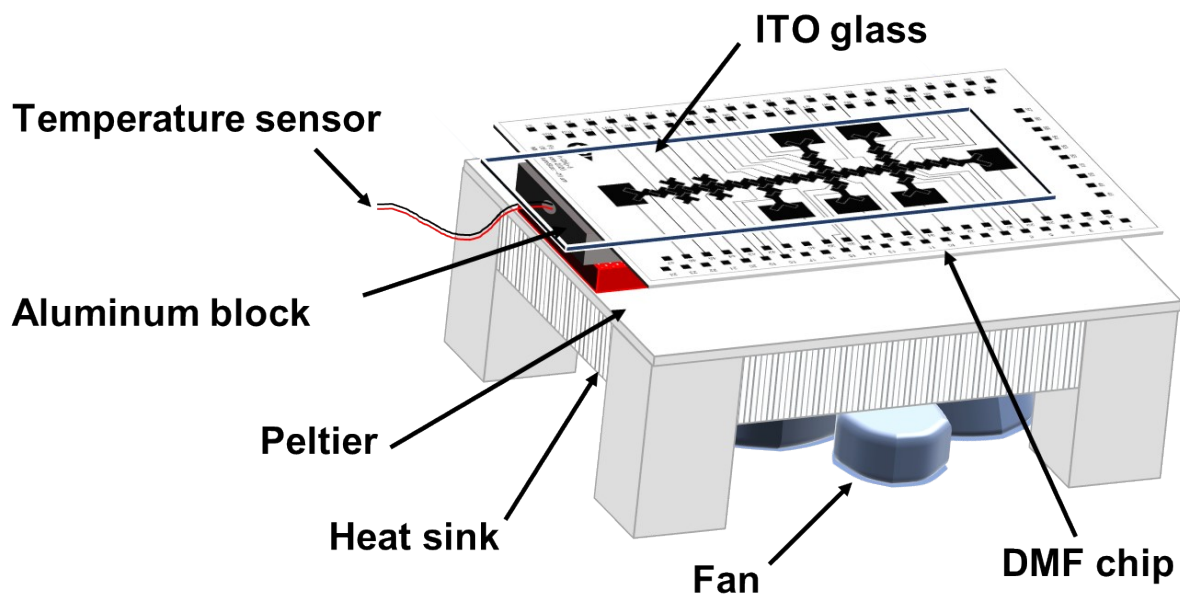


Figure S7: Temperature control module. A thermoelectric device integrated below the DMF device provided heating for the radiosynthesis. A resistance temperature sensor that was inserted in an aluminum block – placed in between device and Peltier for enhancing heat transfer – was used for temperature control. The whole temperate control module with an integrated heatsink and fan was hold with 3D printed holder.

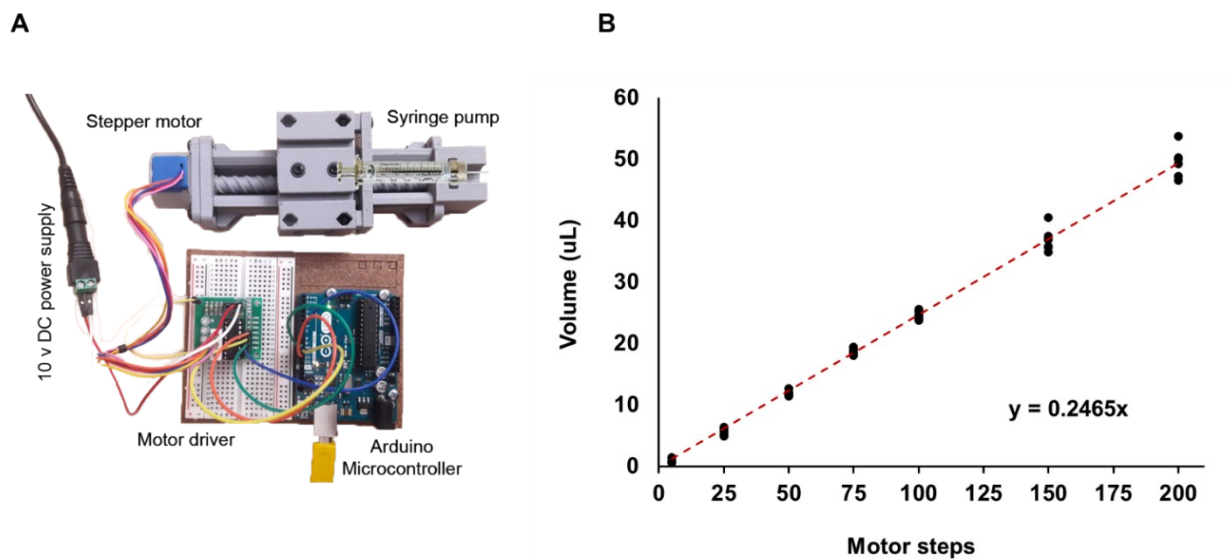


Figure S8: Reagent delivery system. A) The radioisotope was delivered to the reaction site on the DMF device through a tubing connected to a syringe pump. The syringe piston was controlled using a stepper motor and an Arduino microcontroller. B) The calibration curve for the volume dispensed from the tubing versus the stepper motor step angle.

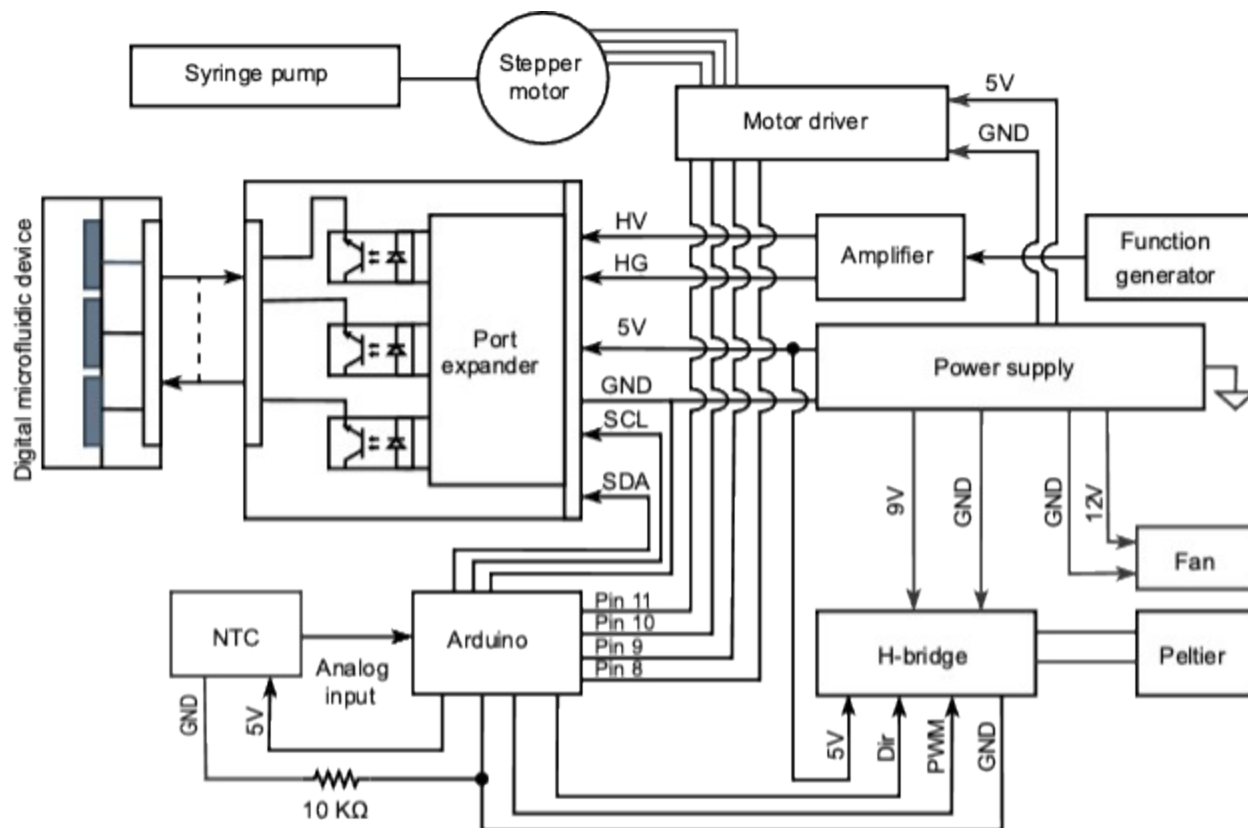


Figure S9: Hardware and software. The control hardware circuit for changing the temperature is previously reported.² Briefly, it consisted of an Arduino microcontroller (Arduino Uno, Italy), a driver motor (consisting of a two half-bridge driver chip and a low resistance N-channel MOSFET) (Amazon, Mississauga, ON, Canada), and the resistance temperature sensor. For the closed-loop control of the heating module, a proportional-integral-derivative (PID) based software code was written in Python v2.7.15. Employing the code, in addition to droplet movement, the user can control the temperature of the reaction site on chip with a tolerance of 3%. The software is open-source and available to download at https://bitbucket.org/shihmicrolab/f_ahmadi_2022.

References

1. Leclerc, L. M. Y.; Soffer, G.; Kwan, D. H.; Shih, S. C. C., A fucosyltransferase inhibition assay using image-analysis and digital microfluidics. *Biomicrofluidics* **2019**, *13* (3), 034106.
2. Moazami, E.; Perry, J. M.; Soffer, G.; Husser, M. C.; Shih, S. C. C., Integration of World-to-Chip Interfaces with Digital Microfluidics for Bacterial Transformation and Enzymatic Assays. *Anal Chem* **2019**, *91* (8), 5159-5168.
3. Perry, J. M.; Soffer, G.; Jain, R.; Shih, S. C. C., Expanding the limits towards ‘one-pot’ DNA assembly and transformation on a rapid-prototype microfluidic device. *Lab on a Chip* **2021**, *21* (19), 3730-3741.
4. Ahmadi, F.; Samlali, K.; Vo, P. Q. N.; Shih, S. C. C., An integrated droplet-digital microfluidic system for on-demand droplet creation, mixing, incubation, and sorting. *Lab on a Chip* **2019**, *19* (3), 524-535.
5. Keng, P. Y.; Chen, S.; Ding, H.; Sadeghi, S.; Shah, G. J.; Dooraghi, A.; Phelps, M. E.; Satyamurthy, N.; Chatziioannou, A. F.; Kim, C. J.; van Dam, R. M., Micro-chemical synthesis of molecular probes on an electronic microfluidic device. *Proc Natl Acad Sci U S A* **2012**, *109* (3), 690-5.
6. Chen, S.; Javed, M. R.; Kim, H. K.; Lei, J.; Lazari, M.; Shah, G. J.; van Dam, R. M.; Keng, P. Y.; Kim, C. J., Radiolabelling diverse positron emission tomography (PET) tracers using a single digital microfluidic reactor chip. *Lab Chip* **2014**, *14* (5), 902-10.
7. Keng, P. Y.; van Dam, R. M., Digital Microfluidics: A New Paradigm for Radiochemistry. *Mol Imaging* **2015**, *14* (12), 13-14.
8. Wang, J.; Chao, P. H.; van Dam, R. M., Ultra-compact, automated microdroplet radiosynthesizer. *Lab Chip* **2019**, *19* (14), 2415-2424.
9. Kohavi, R., A study of cross-validation and bootstrap for accuracy estimation and model selection. In *Proceedings of the 14th international joint conference on Artificial intelligence - Volume 2*, Morgan Kaufmann Publishers Inc.: Montreal, Quebec, Canada, 1995; pp 1137–1143.
10. Chollet, F.; Others, Keras. **2015**.
11. Pedregosa, F.; Varoquaux, G.; Gramfort, A.; Michel, V.; Thirion, B.; Grisel, O.; Blondel, M.; Prettenhofer, P.; Weiss, R.; Dubourg, V.; Vanderplas, J.; Passos, A.; Cournapeau, D.; Brucher, M.; Perrot, M.; Duchesnay, É., Scikit-learn: Machine Learning in Python. *J. Mach. Learn. Res.* **2011**, *12* (null), 2825–2830.